available at www.sciencedirect.com

ScienceDirect

journal homepage: www.elsevier.com/locate/chnjc

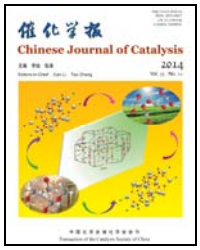

Article

First-principles study of NO reduction by CO on transition metal atoms-doped $CeO_2(111)$

Wuchen Ding, Weixue Li *

State Key Laboratory of Catalysis, Dalian Institute of Chemical Physics, Chinese Academy of Sciences, Dalian 110623, Liaoning, China

ARTICLE INFO

Article history:
Received 16 May 2014
Accepted 10 June 2014
Published 20 December 2014

Keywords:
Nitrogen oxide reduction
Single atom
Single transition metal atom/ceria
Cleavage
Density functional theory plus U

ABSTRACT

We present here a density functional theory plus U study of NO reduction with CO, catalyzed by a single transition metal atom (TM_1 = Zr_1, Tc_1, Ru_1, Rh_1, Pd_1, Pt_1)-doped $CeO_2(111)$. The catalytic center was identified as the TM dopant in combination with lattice oxygen. The investigation into N_2 selectivity focused on three key elementary steps: gaseous N_2O formation, subsequent re-adsorption, and N–O bond scission to produce N_2. In these steps, Rh_1, Pd_1, and $Pt_1/CeO_2(111)$ exhibit a higher selectivity, whereas the other systems (Zr_1, Tc_1, Ru_1) TM_1/CeO_2 show a lower selectivity. The higher selectivity displayed by Pt_1, Pd_1, and Rh_1 dopants arises from the availability of valence *d* electrons, which permit the formation of strong chemical bonds with the reactants and intermediates. Calculated results agree well with experimental findings, and the insights gained can be used to guide the rational design of the doped oxides for catalysis.

© 2014, Dalian Institute of Chemical Physics, Chinese Academy of Sciences.
Published by Elsevier B.V. All rights reserved.

1. Introduction

There is increasing evidence that smaller metal particles dispersed on metal oxides can have superior catalytic activity or selectivity [1–4]. As the metal particle size decreases from nanometers to sub-nanometers, the presence of single metal atoms becomes highly likely. Recent advances in material synthesis methods, surface science, and atomic resolution microscopes [5] provide convincing evidence for the presence of single metal atoms and their role in catalysis [6]. For example, single Pt atoms embedded in the surface of γ-Al_2O_3 [7] and iron oxides [6] were proposed to be responsible for the observed low-temperature oxidation of CO. Moreover, single Pt atoms stabilized by alkali metal ion clusters could catalyze the low-temperature water gas shift reaction (WGS) [8]. Ir was also recently found to have a remarkably high WGS activity when it was atomically dispersed on iron oxides [9]. The atomically dispersed Ir accounted for ~70% of the total catalytic activity, with the remaining activity stemming from sub-nanosized clusters and nanoparticles.

Density functional theory (DFT) has been used to describe catalytic reactions at surfaces in great detail and accuracy and has the great advantage of being able to treat single atom-doped metal oxides in two respects. First, single atom catalysis greatly decreases the complexity of the catalyst structure, which makes it possible to accurately perform simulations using DFT, reducing the well-known material gap between experimental and theoretical studies. Second, the simpler catalyst structure will result in a largely reduced computational cost. There are already some computational reports that suggest that transition metals (such as Mn [10], Ru [11], Pd [12], and Pt [13]) doped into metal oxides (CeO_2 [14], TiO_2 [15], and ZnO [16,17]) could possess additional adsorption sites and a higher oxidation activity for H_2O, CO, CH_4, etc., compared with

* Corresponding author. Tel/Fax: +86-411-84379996; E-mail: wxli@dicp.ac.cn
This work was supported by the National Natural Science Foundation of China (21173210, 21225315), the National Basic Research Program of China (973 Program, 2013CB834603), and the Strategic Priority Research Program of the Chinese Academy of Sciences (XDA09030000).
DOI: 10.1016/S1872-2067(14)60169-8 | http://www.sciencedirect.com/science/journal/18722067 | Chin. J. Catal., Vol. 35, No. 12, December 2014

the undoped metal oxides. Moreover, dopants exhibiting a lower valence state may activate lattice oxygen and lead to lower reaction barriers [18].

NO reduction becomes increasingly important against the background of rapid economic growth. In combustion engines, there are two common technologies for removal of NO under different air-to-fuel ratios: NO_x storage-reduction (NSR) [19–21] in lean-burn engines and selective catalytic reaction (SCR) [22–24] in rich-burn engines. NO reduction by CO, leading to the formation CO_2 and N_2, is a reaction common to both technologies and has the advantage of simultaneously removing two pollutants. To catalyze the reaction, three-way precious metal catalysts including Rh, Pd, or Pt are widely used [22,25,26]. The high cost of these precious metals, however, requires a continuous improvement in atomic efficiency and stability. Recently, atomically dispersed Pd_1, Rh_1, and Pt_1 ions in CeO_2 [26–30] were synthesized in the absence of mixed phases using a solution combustion method [31,32]. These catalysts showed an excellent catalytic activity, selectivity, and stability for the (NO + CO) reaction at low temperature. However, when the dopant is a left-hand transition metals (TM), such as in the $CeZrO_2$ mixed oxide system, a low reduction activity for NO is found, while the catalytic activity for oxidation reactions (CO) is high [33]. Furthermore, $Ce_{0.5}Zr_{0.50}O_2$ was also reported to show a much lower oxygen-storage capacity than $Ce_{0.90}Ru_{0.10}O_{1.94}$ [34]. The reason for the differences in performance is interesting. Theoretical studies of TM-doped ceria focus mainly on understanding CO/NO adsorption [35,36], CO oxidation [10,11,37], CH_4 oxidation [12,13], and CO_2 methanation [38]. Janik et al. [39] studied the stability of Pd-doped ceria using ab initio thermodynamics. They concluded that at 500 K sub-atmospheric partial pressures of oxygen were sufficient to stabilize the Pd_1 atom substituted for the surface Ce sites, whereas at room temperature, oxygen partial pressures above 10^{-10} atm were required.

In our previous work [40], we studied NO reduction by CO on the Pd_1-doped $CeO_2(111)$ surface. The catalytic cycle is summarized in Scheme 1. The reaction center mainly involved the TM dopants associated with lattice oxygen. The main factors that affect the N_2 selectivity of the (NO + CO) reaction on $TM_1/CeO_2(111)$ can be summarized in terms of the TM dopant and the oxygen vacancies. The TM dopants, which possess more *d* electrons than Ce ions, can provide adsorption sites for NO and CO. Oxygen vacancies that are created by CO may help NO undergo conversion into N_2. The major influences on N_2 selectivity can be discerned from examining the following elementary steps. First, oxygen vacancy formation is an elementary step. CeO_2 is a well-known oxygen-storage capacitor (OSC), but whether this ability is enhanced or reduced after introducing the TM dopant requires discussion. The second factor is the complexity of the release of the product N_2O into the gas phase. The formation of gaseous N_2O would lower the selectivity to N_2. The third and final aspect is N_2 formation from N_2O*, where the adsorption configurations of N_2O* require study. Experimental work has shown that Pt- and Rh-doped CeO_2, in addition to Pd, also exhibit promising N_2 selectivities, but the reason for this is unknown. Moreover, whether other TM dopants are active for this catalytic cycle also requires research.

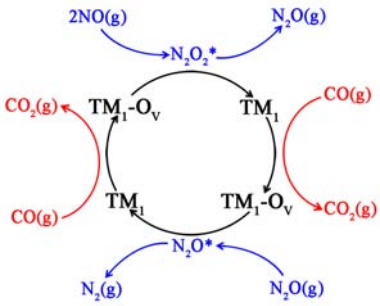

Scheme 1. Catalytic cycle for NO reduction by CO on $TM_1/CeO_2(111)$ surface.

To address the above questions, we performed DFT calculations to study the selectivity to N_2 on Zr_1, Tc_1, Ru_1, Rh_1, Pd_1, and Pt_1-doped $CeO_2(111)$ surfaces. In Section 3.1, CO oxidation on $TM_1/CeO_2(111)$ is discussed; in Section 3.2, the transition from N_2O_2* to gaseous N_2O on $TM_1/CeO_2(111)$ is presented; and in Section 3.3, the N_2O adsorption configurations on $TM_1/CeO_2(111)$ surfaces with oxygen vacancies are treated. Finally, in Section 3.4, the second N–O bond scission during the reduction of N_2O to N_2 is examined.

2. Theoretical approaches and computational details

Spin-polarized total energy calculations were performed based on the all-electron projected augmented wave (PAW) method and DFT+U methodology, within the generalized gradient approximation (GGA-PW91) functional as implemented in the Vienna Ab Initio Simulation Package (VASP) [41–45]. A cutoff of 400 eV was used for the plane wave expansion. U = 5 eV was applied to Ce 4*f* states in line with previous calculations [12,35,46]. The oxide surface was modeled via a $CeO_2(111)$-p(3×3) supercell with a thickness of three O-Ce-O tri-layers (27 Ce atoms and 54 O atoms in total) separated by a 15 Å vacuum. For the surface Brillouin zone sampling, we employed a Monkhorst-Pack (1×1×1) Γ-centered k-points grid [37,47]. The calculation based on the Monkhorst-Pack of (2×2×1) lowers the total energy by less than 0.02 eV. The top two tri-layers and the adsorbates were relaxed until the residual force on each ion was less than 0.02 eV/Å.

To simulate Zr_1, Tc_1, Ru_1, Rh_1, Pd_1, and $Pt_1/CeO_2(111)$ catalysts, one surface Ce cation was substituted by a single Zr_1, Tc_1, Ru_1, Rh_1, Pd_1, or Pt_1 atom (Fig. 1). All adsorptions and reactions were performed on one side of the exposed surface with the transition metal dopant, and a dipole moment correction along the *z*-direction was applied. The climbing-image nudged elastic

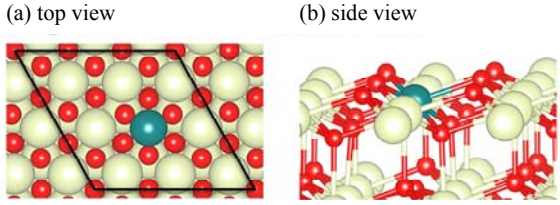

Fig. 1. Top (a) and side (b) view of slab models for $TM_1/CeO_2(111)$. The TM_1 dopant is located at a surface Ce site (blue). The gray and red spheres represent a Ce atom and an O atom, respectively.

band (CI-NEB) method [48,49] was used to search the transition states (TSs) for all the elementary reactions studied. The minimum energy pathway for each elementary reaction was discretized by a total of six images between the initial and final states. The TS was denoted by the highest amplitude image along the minimum energy path. The activation energy (E_a) of each elementary reaction was calculated by the Born-Oppenheimer energy difference between the TS and the initial state (IS) without including zero-point energy contributions.

3. Results and discussion

3.1. CO oxidation

The calculated lattice parameter of bulk CeO_2 was 5.49 Å, which agrees well with previous calculations [50]. In this study we use the $CeO_2(111)$ surface as the support because it is the most abundant surface facet exposed on pristine CeO_2 [51]. Each surface Ce atom coordinates with seven oxygen atoms, and the optimized Ce–O bond length is 2.37 Å. The calculated formation energy of an isolated TM_1 atom occupying a pre-existing Ce vacancy is highly exothermic with a value of –20.73 eV (Zr_1), –15.23 eV (Tc_1), –12.75 eV (Ru_1), –10.09 eV (Rh_1), –7.34 eV (Pd_1), and –9.65 eV (Pt_1). This suggests that the substituted TM_1 atom is stable and would be resistant to segregation and agglomeration toward larger metal particles. The high coordination number of a substituted TM_1 atom with lattice oxygen O_L is decisive for its stability and cationic charge state.

The complete phase diagram of Pd-$CeO_2(111)$ under relevant conditions was studied thoroughly by Janik et al. [39] using ab initio thermodynamics. In that work, a number of configurations including Pd_1 adatoms on $CeO_2(111)$, Pd_1 substituted at the surface Ce sites, the subsurface sites, and Pd_4 clusters were studied, and their relative stabilities with respect to Pd bulk metal and oxides were compared. They found that Pd could form single adatoms on the surface or substitute with the surface Ce sites under a wide range of oxygen chemical potentials. Accordingly, the TM_1 atom substituted at the surface Ce sites is used in the present work unless stated otherwise.

As shown in Scheme 1, the catalytic center for NO reduction by CO involves a cycle between the single transition metal (TM_1) and the TM_1 with an adjacent oxygen vacancy (TM_1-O_V). Oxygen vacancy (O_V) formation has a crucial impact on the integrity and sustainability of the reaction. The computed O_V formation energies (E_V) and the reaction energies (E_r) are listed in Table 1.

The calculated energy of formation (E_V) of O_V on the $CeO_2(111)$ surface with respect to gas phase O_2 is 2.10 eV (endothermic), which is in good agreement with previous reports [52,53]. This indicates the higher activity of the lattice oxygen O_L and the higher reducibility of $CeO_2(111)$. The calculated O_V formation energies on each $TM_1/CeO_2(111)$ system considered are 1.48 eV (Zr_1), 1.20 eV (Tc_1), 1.00 eV (Ru_1), 1.15 eV (Rh_1), 0.65 eV (Pd_1), and 1.43 eV (Pt_1). All the O_V formation energies for $TM_1/CeO_2(111)$ exhibit a considerably reduced value compared with $CeO_2(111)$ (2.10 eV), which indicates that the lattice oxygen becomes more active after TM_1 dopant introduction .

Table 1
Oxygen vacancy formation energy (E_V) and CO oxidation reaction energy (E_r) on the various $TM_1/CeO_2(111)$ surfaces.

TM	Ideal	Zr	Tc	Ru	Rh	Pd	Pt
E_V (eV)	2.10	1.48	1.20	1.00	1.15	0.65	1.43
E_r (eV)	–1.14	–1.80	–2.09	–2.29	–2.14	–2.63	–1.86

Our previous work [40] reported that the barrier for CO reacting with O_L on Pd_1-doped $CeO_2(111)$ (0.11 eV) was lower than that on $CeO_2(111)$ (0.42 eV) through the Eley-Rideal (E-R) type of reaction mechanism. Moreover, the reaction energies reveal that this step is highly exothermic, taking values of –1.80 eV (Zr_1), –2.09 eV (Tc_1), –2.29 eV (Ru_1), –2.14 eV (Rh_1), –2.63 eV (Pd_1), and –1.86 eV (Pt_1). The minimum E_r (–1.80 eV on Zr_1) is more exothermic than that on $CeO_2(111)$ (–1.14 eV). We can infer that the barrier for CO oxidation on the $TM_1/CeO_2(111)$ surface is lower than that found for $CeO_2(111)$ (0.42 eV).

The formation energies of oxygen vacancies on the $TM_1/CeO_2(111)$ systems studied here are all lower than that of $CeO_2(111)$, and the reaction energies are all higher than that of $CeO_2(111)$. We can infer that CO oxidation with O_L to create an O_V on Zr_1, Tc_1, Ru_1, Rh_1, Pd_1, and $Pt_1/CeO_2(111)$ is a facile step, and oxygen vacancies are available during the whole reaction, an important requisite in our mechanism.

3.2. Formation of N_2O_2* and N_2O

Having shown that oxygen vacancies can be available during the whole reaction, we now turn to studying NO reduction on a TM_1-O_V center, as O_V can act as an oxygen acceptor during N–O bond scission. To test the possibility of direct NO dissociation, the dissociative reaction energy from gas phase NO to N* and O* adsorbed at a cation-top was investigated. For stoichiometric $CeO_2(111)$ and $Pd_1/CeO_2(111)$, the calculated reaction energies are highly endothermic (> 6 eV). Even for the reduced surfaces where the presence of O_V might accommodate the dissociated O*, the reaction energies remain very endothermic at 1.95 eV for $O_V/CeO_2(111)$ and 3.54 eV for Pd_1-$O_V/CeO_2(111)$. These results indicate that direct NO dissociation into N* and O* can hardly contribute to N_2 formation, if at all, on either stoichiometric or reduced $CeO_2(111)$ and $TM_1/CeO_2(111)$.

Alternatively, N_2 formation might arise from the formation of the N_2O_2* intermediate from two NO* molecules adsorbed on the surface, followed by the subsequent scission of the N–O bonds. As shown schematically in Fig. 2(a) and (b), N_2O_2* prefers to bind to the TM_1-O_V pairs, one binding via the N atom (N(1)) to a TM_1-top site and the other binding via the O atom (O(2)) to an O_V adjacent to the TM_1 atom. The formation energies of N_2O_2* (E_N) with respect to (NO+NO) in the gas phase (Table 2) on Zr_1, Tc_1, Ru_1, Rh_1, Pd_1, and $Pt_1/CeO_2(111)$ are –2.27, –1.87, –2.38, –3.10, –2.88, and –3.55 eV, respectively. The E_N values of $TM_1/CeO_2(111)$ considered are all much higher than that of trans-N_2O_2 in the gas phase (–0.71 eV). This reveals that N_2O_2* tends to form on the TM_1-O_V site and the N–N binding energy is only one part of the E_N value on the TM_1-O_V/$CeO_2(111)$ surface. Moreover, the reaction barriers for the formation of N_2O_2*, which were also estimated, are small and sometimes negligible.

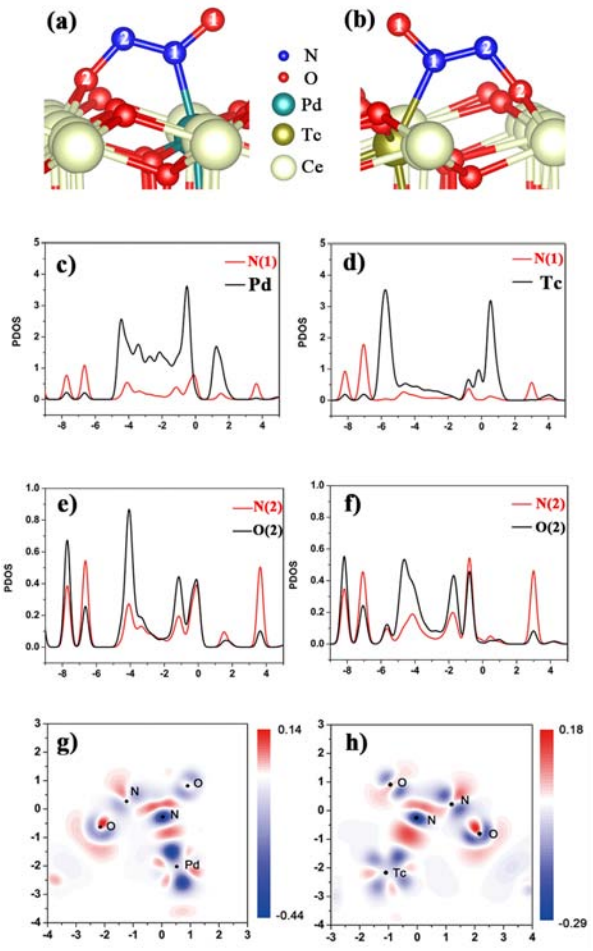

Fig. 2. Adsorption structure of N_2O_2* on Pd_1-O_V/CeO_2(111) (a) and N_2O_2* on Tc_1-O_V/CeO_2(111) (b). Side view of the charge density difference distribution of N_2O_2* on Pd_1-O_V/CeO_2(111) (c) and N_2O_2* on Tc_1-O_V/CeO_2(111) (d). The red profile denotes the electron gains, and the blue profile indicates the electron loss (values in e/Å^3). Projected density of states (PDOS) of TM_1 with N(1) of N_2O_2* on Pd_1-O_V/CeO_2(111) (e) and Tc_1-O_V/CeO_2(111) (f) and O(2) with N(2) of N_2O_2* on Pd_1-O_V/CeO_2(111) (g) and Tc_1-O_V/CeO_2(111) (h).

The decomposition of N_2O_2* into N_2O requires the scission of the TM–N and O–N bond. Sequential or simultaneous scission of these two bonds indicates two potential reaction pathways for this elementary step. We have studied these two pathways on Pd_1/CeO_2(111) in our previous work [40], and the two effective activation barriers are comparable (1.85 versus 1.96 eV). For simplicity, we investigated the simultaneous dissociation of the TM–N and O–N bonds for the TM_1/CeO_2(111) system. Calculated activation barriers and reaction energies for the conversion of N_2O_2* to gaseous N_2O are summarized in Fig. 3. Calculated barriers for Zr_1, Tc_1, Ru_1, Rh_1, Pd_1, and Pt_1/CeO_2(111) are 1.01, 0.07, 0.88, 1.89, 1.96, and 2.05 eV, respectively. The reaction energies for Zr_1, Tc_1, and Ru_1/CeO_2(111) are exothermic with values of –1.08, –1.43, and –1.06 eV, respectively. In contrast, the values for Rh_1, Pd_1, and Pt_1/CeO_2(111) are endothermic with values of 0.06, 0.34, and 0.22 eV, respectively. As shown in Fig. 3, there is a strong correlation between calculated activation barriers and reaction energies due to the similar TS structures. The desorption of N_2O into the gas phase is facile on the left-hand elements in the periodic table, i.e. Zr_1, Tc_1, and Ru_1/CeO_2 (111). The further to the right the dopants are in the periodic table, the more difficult it is for N_2O desorption to occur, e.g. gaseous N_2O formation on Rh_1, Pd_1, and Pt_1/CeO_2(111) has a higher activation barrier than the other metals studied.

Table 2
Formation energy of N_2O_2* (E_N) on the TM_1-O_V/CeO_2(111) surfaces and the adsorption energy for the N_2O bent configuration (E_{ad}).

TM	Zr	Tc	Ru	Rh	Pd	Pt
E_N (eV)	–2.27	–1.87	–2.38	–3.10	–2.88	–3.55
E_{ad} (eV)	0.13	0.70	–0.01	–0.42	–0.56	–1.12

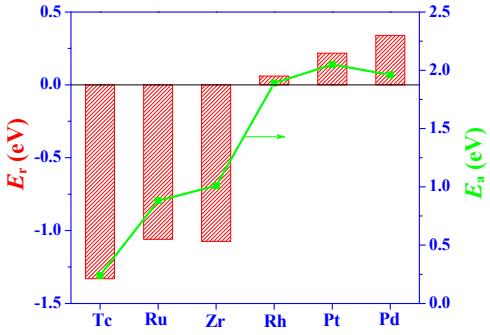

Fig. 3. Correlation between the reaction barrier and the reaction energy in the desorption of N_2O on TM_1/CeO_2(111) surfaces.

To understand the underlying differences for N_2O formation on different TM_1/CeO_2(111) systems, charge density difference distribution analysis and site-projected density of states (PDOS) calculations were performed on Pd_1/CeO_2(111) (Fig. 2(a)) and Tc_1/CeO_2(111) (Fig. 2(b)). The charge density difference distribution shows that N_2O_2* on Pd_1-O_V/CeO_2(111) (Fig. 2(c)) and Tc_1-O_V/CeO_2(111) (Fig. 2(d)) has similar bonding structures, with a pronounced charge accumulation between Pd_1/Tc_1 and N_2O_2* and a redistribution around Pd_1/Tc_1 and N_2O_2*. However, charge density differences also show that redistribution decreases for Pd more significantly than for Tc.

In addition, PDOS calculations show that there are differences in the electronic structures between N(1)-Pd and N(1)-Tc, (Fig. 2(e) and (f)). For N_2O_2* at Pd_1-O_V/CeO_2(111), Pd 4*d*-electrons dominate the PDOS below the Fermi level. The comprehensive orbital hybridization with the N_2O_2 orbital [54], and formation of bonding and antibonding states below and above the Fermi level, are evident. Compared with N(1) and Tc, there is a higher more orbital overlap between the N(1) and Pd, which implies that the Pd-N bond is stronger than the Tc-N bond. For comparison, calculated PDOS results of N(2) and O(2) (Fig. 2(g) and (h)) indicate that the electronic structures of the N–O bond of N_2O_2* on Pd_1/CeO_2(111) and Tc_1/CeO_2(111) are very similar. Because both the TM–N and the O–N bonds must dissociate for the formation of gaseous N_2O, the bond energy of TM–N can correspond to the relevant activated reaction barrier.

In summary, N_2O is easy to desorb into gas phase on left-hand TM_1/CeO_2(111) systems, while on the right-hand transition metals Rh_1, Pd_1, and Pt_1/CeO_2(111), N_2O binds more

strongly and is therefore less likely to desorb. Because the desorption of reactants is unfavorable for the subsequent reduction steps, Rh_1, Pd_1, and $Pt_1/CeO_2(111)$ with lower desorption energies may have a higher N_2 selectivity than the right $TM_1/CeO_2(111)$.

3.3. Re-adsorption of gaseous N_2O

As discussed above, N_2O is easily formed and can readily desorb into the gas phase on Zr_1, Tc_1, and $Ru_1/CeO_2(111)$. Although N_2O desorption is difficult on Rh_1, Pd_1, and $Pt_1/CeO_2(111)$, there may be some gaseous N_2O released during the reaction. As the reduction of N_2O to N_2 requires the TM_1-O_V site, the re-adsorption of gaseous N_2O is an essential step for N_2 formation. In this section, we focus on N_2O re-adsorption at the TM_1-O_V center.

There are two possible N_2O adsorption configurations on TM_1-$O_V/CeO_2(111)$ surfaces: a bending mode and a linear form. The calculated adsorption energies of these two configurations for all the $TM_1/CeO_2(111)$ systems studied are shown in Fig. 4. For linearly adsorbed N_2O (Fig. 4(b), red frame), the O atom binds with O_V and the terminal N atom is oriented to the vacuum. The calculated adsorption energy for the linear configuration is small, typical of physical adsorption, with values in the range from 0.15 to –0.27 eV. The bent adsorbed state (Fig. 4(c), black frame) binds through both N and O at the TM_1 site and O_V site of TM_1-$O_V/CeO_2(111)$, respectively. The corresponding adsorption energies for Zr_1, Tc_1, and Ru_1 are endothermic with values of 0.13, 0.56, and 0.01 eV, respectively, whereas the values are exothermic at –0.42, –0.56, and –1.12 eV for Rh_1, Pd_1, and Pt_1, respectively.

To elucidate the reasons for the differences between the bent N_2O adsorption at the various TM_1-O_V centers, we separate the bent adsorption energy into two parts: the endothermic deformation energy (E_d) (conversion of the linear configuration to a bent configuration) and a binding energy (E_b) between the bent configuration and the TM_1-O_V center, an exothermic process. The calculated adsorption energy of N_2O on Pd_1-O_V/CeO_2 (E_{ad} = –0.56 eV) is separated into 2.02 eV (E_d) and –2.58 eV (E_b), while for Zr_1-O_V/CeO_2 (E_{ad} = 0.13 eV) the values are 1.99 eV (E_d) and –1.86 eV (E_b). The deformation energy is comparable for Pd and Zr because of the similar bent configuration of N–N–O: 129.8° (Pd) and 130.3° (Zr). However, the binding strength of Pd is much higher than that of Zr, which is responsible for an endothermic E_{ad} value for Zr and an exothermic value for Pd. Similar results were also found for Pt and Tc, i.e., the deformation energy and the N–N–O angle are comparable (2.88 versus 2.70 eV and 122.2° versus 122.4°). The binding strength of Pt (–3.99 eV) is much higher than that of Tc (–2.01 eV). When the binding energy could not compensate for the bending energy, the overall adsorption energy exhibited a positive value.

As discussed in Section 3.2, left-hand TMs have weak bonding with the N, whereas the right-hand TMs bind more strongly. As a result, the stronger binding of Rh_1, Pd_1, and $Pt_1/CeO_2(111)$ with N can compensate for the bending energy of N_2O, whereas Zr_1, Tc_1, and $Ru_1/CeO_2(111)$ do not bind to N with sufficient strength to compensate for the bending energy. Our DFT computations reveal that re-adsorption of gaseous N_2O on TM_1-O_V is weak on the left-hand $TM_1/CeO_2(111)$, and that linear physisorption is the preferred mode of adsorption. In contrast, stronger bent chemisorption of N_2O is stable for Rh_1, Pd_1, and $Pt_1/CeO_2(111)$, which would then exhibit higher N_2 selectivities than Zr_1, Tc_1, and $Ru_1/CeO_2(111)$.

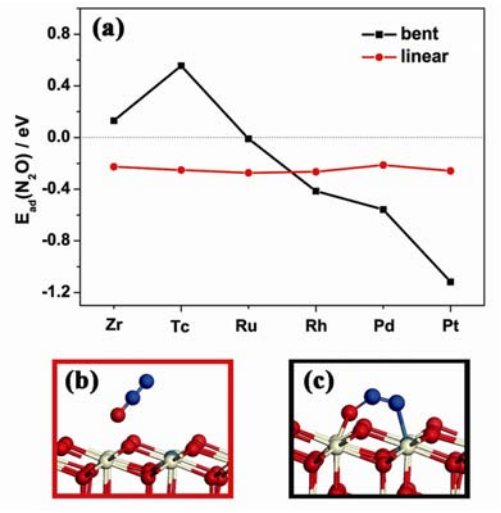

Fig. 4. (a) Adsorption energies of gaseous N_2O on reduced TMs doped-$CeO_2(111)$ surfaces with bent (black) and linear (red) configurations, respectively; N_2O adsorption on Pd_1-$O_V/CeO_2(111)$ with linear (b) and bent (c) configurations, respectively.

3.4. The formation of N_2

In the above section, we examined the elementary steps of gaseous N_2O formation and N_2O re-adsorption (essential for N_2 formation) at TM_1-O_V centers from the viewpoints of both kinetics and energetics. Having studied the adsorption configurations of N_2O on TM_1-$O_V/CeO_2(111)$ surfaces, we addressed the two competing pathways for the reduction and desorption of N_2O*. Calculated barriers for N–O bond scission and the desorption energy of N_2O* for each TM are presented in Fig. 5(a). It is clear that the barriers for gaseous N_2 formation on Zr_1, Tc_1, and $Ru_1/CeO_2(111)$ with a linear N_2O configuration are larger than the N_2O desorption energies (0.23, 0.25, and 0.27 eV for Zr_1, Tc_1, and Ru_1, respectively). This implies that N_2O* desorption is easier than its reduction for these systems. In contrast, for Rh_1, Pd_1, and $Pt_1/CeO_2(111)$, the desorption energies of N_2O with a bent configuration (0.42, 0.56, and 1.12 eV for Rh_1, Pd_1, and Pt_1, respectively) are larger than the reduction barriers (0.04, 0.24, and 0.03 eV for Rh_1, Pd_1, and Pt_1, respectively). This suggests that the reduction process proceeds more easily than desorption.

The reduction barrier from the initial bent state is lower than that from the linear initial state. There are differences in the N–O bond lengths between the linear and bent states, and this influences the reaction barrier. The N_2O linear adsorbed state has an N–O bond length of 1.21 Å (Zr), almost equal to that of gaseous N_2O (1.14 Å). However, for N_2O bent adsorption, the N–O bond length is elongated by 0.14 Å compared with

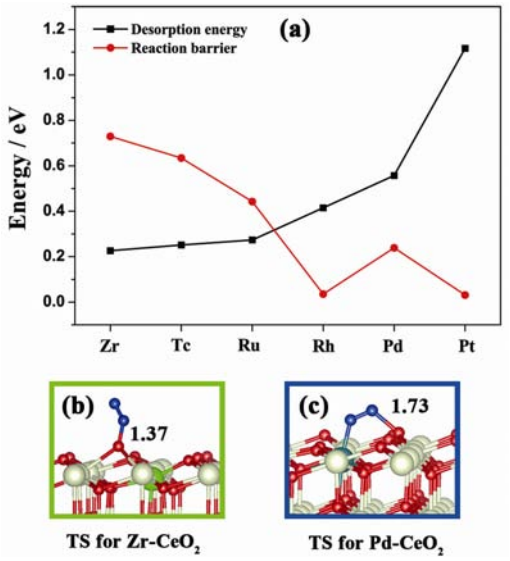

Fig. 5. (a) Correlations between calculated barriers (red) for N_2O reduction and desorption energies (black) of N_2O on TM_1-O_V/CeO_2(111); (b) The transition structure of linear N_2O reduction on Zr_1-O_V/CeO_2(111); (c) The transition structure of bent N_2O reduction on Pd_1-O_V/CeO_2(111).

the linear adsorbed state, and this leads to the higher activity of the N–O bond in the bent configuration. The smaller angle of N–N–O in the bent configuration (130°) compared with the linear configuration (180°) also helps to preactivate the N–N–O bond.

For the initial state with the linear configuration, the transition state structure on Zr_1/CeO_2(111) is shown in Fig. 5(b). The configurations of TSs for Tc_1 and Ru_1 doped CeO_2(111) are similar to that for TM = Zr_1. In the TS for linear adsorption, the bond length of N–O is elongated by 0.16 Å, and the O atom almost completely moves into the O vacancy site. For the initial state with the bent configuration, the structure of the transition state for TM = Rh_1 or Pt_1 is similar to that for Pd_1/CeO_2(111) (Fig. 5(c)). In the TS for bent adsorption, the bond length of N–O is elongated by 0.38 Å, more than that of the linearly adsorbed state. In general, the bent adsorption configuration possesses a lower reduction barrier than that found with linear adsorption. CeO_2(111) doped left-hand TMs can only achieve linear adsorption, while in the case of right-hand TMs, the bent adsorption structure is preferred, and the selectivity of N_2 is higher for the right-hand elements on CeO_2(111).

In summary, for Zr_1, Tc_1, and Ru_1/CeO_2, gaseous N_2O is formed easily, and the preferential re-adsorption configuration at TM_1-O_V involves linear physisorption. Moreover, the reduction barrier of N_2O* is larger than that of desorption. All three aspects result in a lower N_2 selectively, which agrees well with the experiment work [33], where cerium/zirconium mixed oxides were found to exhibit a small reduction activity for NO. In contrast, for TMs = Rh_1, Pd_1, or Pt_1/CeO_2(111), N_2O desorbs with difficulty. In addition, the gaseous N_2O can easily adsorb on TM_1-O_V with the bent configuration, and the adsorption energies are larger than the reaction barriers to N_2 formation. Overall, our results for Rh_1, Pd_1, and Pt_1/CeO_2(111) are in good agreement with the experimental studies [26,28,55], where excellent catalytic activity, selectivity, and stability for the NO+CO reaction at low temperature have been demonstrated for Rh-, Pd-, and Pt-doped CeO_2.

4. Conclusions

The N_2 selectivity of the NO+CO reaction on single transition metal (TM = Zr_1, Tc_1, Ru_1, Rh_1, Pd_1, and Pt_1) atom-doped CeO_2(111) surfaces was investigated using density functional theory. The catalytic center was identified as the TM dopant in interaction with lattice oxygen. The study of N_2 selectivity focused on three critical elementary steps: gaseous N_2O formation, subsequent N_2O re-adsorption, and formation of N_2. The calculations predict that Rh_1, Pd_1, and Pt_1/CeO_2(111) would exhibit a higher N_2 selectivity, whereas the left-hand TM_1/CeO_2 systems would have a lower N_2 selectivity, all consistent with available experimental results. The origin of the high N_2 selectivity for Rh_1, Pd_1, and Pt_1/CeO_2(111) stems from the availability of *d* valence electrons because this permits the formation of strong chemical bonds with the reactants and intermediates involved in the reaction.

References

[1] Herzing A A, Kiely C J, Carley A F, Landon P, Hutchings G J. *Science,* 2008, 321: 1331
[2] Turner M, Golovko V B, Vaughan O P H, Abdulkin P, Berenguer-Murcia A, Tikhov M S, Johnson B F G, Lambert R M. *Nature,* 2008, 454: 981
[3] Vajda S, Pellin M J, Greeley J P, Marshall C L, Curtiss L A, Ballentine G A, Elam J W, Catillon-Mucherie S, Redfern P C, Mehmood F, Zapol P. *Nat Mater,* 2009, 8: 213
[4] Judai K, Abbet S, Wörz A S, Heiz U, Henry C R. *J Am Chem Soc,* 2004, 126: 2732
[5] Liu J Y. *ChemCatChem,* 2011, 3: 934
[6] Qiao B T, Wang A Q, Yang X F, Allard L F, Jiang Z, Cui Y T, Liu J Y, Li J, Zhang T. *Nat Chem,* 2011, 3: 634
[7] Kwak J H, Hu J Z, Mei D H, Yi C W, Kim D H, Peden C H F, Allard L F, Szanyi J. *Science,* 2009, 325: 1670
[8] Zhai Y P, Pierre D, Si R, Deng W L, Ferrin P, Nilekar A U, Peng G W, Herron J A, Bell D C, Saltsburg H, Mavrikakis M, Flytzani-Stephanopoulos M. *Science,* 2010, 329: 1633
[9] Lin J, Wang A Q, Qiao B T, Liu X Y, Yang X F, Wang X D, Liang J X, Li J, Liu J Y, Zhang T. *J Am Chem Soc,* 2013, 135: 15314
[10] Hsu L C, Tsai M K, Lu Y H, Chen H T. *J Phys Chem C,* 2013, 117: 433
[11] Chen H T. *J Phys Chem C,* 2012, 116: 6239
[12] Mayernick A D, Janik M J. *J Catal,* 2011, 278: 16
[13] Tang W, Hu Z P, Wang M J, Stucky G D, Metiu H, McFarland E W. *J Catal,* 2010, 273: 125
[14] Chen H T, Chang J G. *J Phys Chem C,* 2011, 115: 14745
[15] Chrétien S, Metiu H. *Catal Lett,* 2006, 107: 143
[16] Gu X K, Ding W C, Huang C Q, Li W X. *Chin J Catal* (顾向奎, 丁戊辰, 黄传奇, 李微雪. 催化学报), 2012, 33: 1427
[17] Yao K, Wang S S, Gu X K, Su H Y, Li W X. *Chin J Catal* (姚锟, 王莎莎, 顾向奎, 苏海燕, 李微雪. 催化学报), 2013, 34: 1705
[18] McFarland E W, Metiu H. *Chem Rev,* 2013, 113: 4391
[19] Liu G, Gao P X. *Catal Sci Technol,* 2011, 1: 552
[20] Liu Z M, Woo S I. *Catal Rev-Sci Eng,* 2006, 48: 43
[21] Epling W S, Campbell L E, Yezerets A, Currier N W, Parks J E. *Catal Rev-Sci Eng,* 2004, 46: 163

Graphical Abstract

Chin. J. Catal., 2014, 35: 1937–1943 doi: 10.1016/S1872-2067(14)60169-8

First-principles study of NO reduction by CO on transition metal atoms-doped CeO_2(111)

Wuchen Ding, Weixue Li*
Dalian Institute of Chemical Physics, Chinese Academy of Sciences

Right transition metal (TM)-doped CeO_2(111) possesses high N_2 selectivity because of the right-hand TMs being able to provide more *d* electrons for stronger binding between the TM and N-containing species. For the left-hand TMs, *d* electron availability is lower, leading to a weaker binding situation and lower N_2 selectivity.

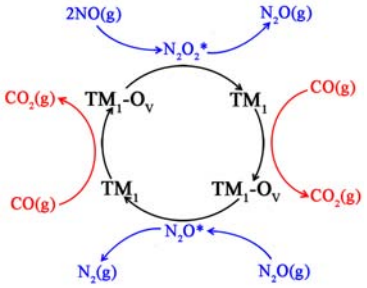

[22] Srinivasan A, Depcik C. *Catal Rev-Sci Eng,* 2010, 52: 462
[23] Burch R, Breen J P, Meunier F C. *Appl Catal B,* 2002, 39: 283
[24] Liu Z M, Woo S I, Lee W S. *J Phys Chem B,* 2006, 110: 26019
[25] Pisanu A M, Gigola C E. *Appl Catal B,* 1999, 20: 179
[26] Bera P, Patil K C, Jayaram V, Subbanna G N, Hegde M S. *J Catal,* 2000, 196: 293
[27] Hegde M S, Madras G, Patil K C. *Acc Chem Res,* 2009, 42: 704
[28] Roy S, Hegde M S. *Catal Commun,* 2008, 9: 811
[29] Roy S, Marimuthu A, Hegde M S, Madras G. *Appl Catal B,* 2007, 71: 23
[30] Priolkar K R, Bera P, Sarode P R, Hegde M S, Emura S, Kumashiro R, Lalla N P. *Chem Mater,* 2002, 14: 2120
[31] Patil K C, Aruna S T, Ekambaram S. *Curr Opin Solid State Mater Sci,* 1997, 2: 158
[32] Patil K C, Aruna S T, Mimani T. *Curr Opin Solid State Mater Sci,* 2002, 6: 507
[33] González-Velasco J R, Gutiérrez-Ortiz M A, Marc J L, Botas J A, González-Marcos M P, Blanchard G. *Appl Catal B,* 1999, 22: 167
[34] Singh P, Hegde M S. *Chem Mater,* 2009, 21: 3337
[35] Yeriskin I, Nolan M. *J Chem Phys,* 2009, 131: 244702
[36] Nolan M. *J Phys Chem C,* 2009, 113: 2425
[37] Nolan M. *J Chem Phys,* 2009, 130: 144702
[38] Sharma S, Hu Z P, Zhang P, McFarland E W, Metiu H. *J Catal,* 2011, 278: 297
[39] Mayernick A D, Janik M J. *J Chem Phys,* 2009, 131: 084701
[40] Ding W C, Gu X K, Su H Y, Li W X. *J Phys Chem C,* 2014, 118: 12216
[41] Kresse G, Joubert D. *Phys Rev B,* 1999, 59: 1758
[42] Kresse G, Furthmuller J. *Comput Mater Sci,* 1996, 6: 15
[43] Kresse G, Furthmuller J. *Phys Rev B,* 1996, 54: 11169
[44] Kresse G, Hafner J. *Phys Rev B,* 1994, 49: 14251
[45] Kresse G, Hafner J. *Phys Rev B,* 1993, 48: 13115
[46] Nolan M. *J Mater Chem,* 2011, 21: 9160
[47] Shapovalov V, Metiu H. *J Catal,* 2007, 245: 205
[48] Henkelman G, Uberuaga B P, Jonsson H. *J Chem Phys,* 2000, 113: 9901
[49] Henkelman G, Jonsson H. *J Chem Phys,* 2000, 113: 9978
[50] Yang Z X, Woo T K, Hermansson K. *Surf Sci,* 2006, 600: 4953
[51] Skorodumova N V, Baudin M, Hermansson K. *Phys Rev B,* 2004, 69: 075401
[52] Li H Y, Wang H F, Gong X Q, Guo Y L, Guo Y, Lu G Z, Hu P. *Phys Rev B,* 2009, 79: 193401
[53] Ganduglia-Pirovano M, Da Silva J L F, Sauer J. *Phys Rev Lett,* 2009, 102: 026101
[54] Zeng Z H, Da Silva J L F, Li W X. *Phys Chem Phys Chem,* 2010, 12: 2459
[55] Bera P, Hegde M S. *Catal Surv Asia,* 2011, 15: 181

过渡金属替代的CeO_2(111)表面上NO+CO反应机理的理论研究

丁戊辰, 李微雪*
中国科学院大连化学物理研究所, 辽宁大连116023

摘要: 采用DFT+U方法研究了过渡金属替代的CeO_2(111)表面上的NO+CO反应机理, 以探求不同过渡金属对N_2选择性的影响. 结果表明, 在反应过程中, 反应活性中心由过渡金属单原子与其最近邻的氧空位组成. NO在过渡金属-氧空位上发生N–O断键, 不同过渡金属上该还原步骤的难易程度不同. 计算发现, 右过渡金属Rh, Pd和Pt替代的CeO_2(111)表面可以与吸附物之间形成较强的吸附作用, 进而可以达到较高的N_2选择性. 其主要原因是右过渡金属具有较多的*d*电子, 可以与吸附小分子之间形成有效的反馈键. 而左过渡金属拥有较少的*d*电子, 难以有效抓住吸附物, 最终导致较低的N_2选择性.

关键词: 一氧化氮消除; 选择性; 单原子; 单过渡金属原子/氧化铈; 密度泛函理论+U

收稿日期: 2014-05-16. 接受日期: 2014-06-10. 出版日期: 2014-12-20.
*通讯联系人. 电话/传真: (0411)84379996; 电子信箱: wxli@dicp.ac.cn
基金来源: 国家自然科学基金(21173210, 21225315); 国家重点基础研究发展计划(973计划, 2013CB834603); 中国科学院战略性先导科技专项(XDA09030000).
本文的英文电子版由Elsevier出版社在ScienceDirect上出版(http://www.sciencedirect.com/science/journal/18722067).